Transparent Dual-Frequency CMUT Arrays for Photoacoustic Imaging

Mahyar Ghavami, *Graduate Student Member, IEEE*,
Mohammad Rahim Sobhani, *Graduate Student Member, IEEE*,
and Roger Zemp, *Member, IEEE*

***Abstract*—The opaque ultrasound transducers used in conventional photoacoustic imaging systems necessitate oblique light delivery, which gives rise to some disadvantages such as inefficient target illumination and bulky system size. This work proposes a transparent capacitive micromachined ultrasound transducer (CMUT) linear array with dual-band operation for through-illumination photoacoustic imaging. Fabricated using an adhesive wafer bonding method, the array consists of optically transparent conductors [indium tin oxide (ITO)] as both top and bottom electrodes, a transparent polymer [bis-benzocyclobutene (BCB)] as the sidewall and adhesive material, and largely transparent silicon nitride as the membrane. The fabricated device had a maximum optical transparency of 76.8% in the visible range. Furthermore, to simultaneously maintain higher spatial resolution and deeper imaging depth, this dual-frequency array consists of low- and high-frequency channels with 4.2- and 9.3-MHz center frequencies, respectively, which are configured in an interlaced architecture to minimize the grating lobes in the receive point spread function (PSF). With a wider bandwidth compared to the single-frequency case, the fabricated transparent dual-frequency CMUT array was used in through-illumination photoacoustic imaging of wire targets demonstrating an improved spatial resolution and imaging depth.**

***Index Terms*—Capacitive micromachined ultrasound transducers (CMUTs), dual-frequency transducer, photoacoustic imaging, through illumination, transparent transducer.**

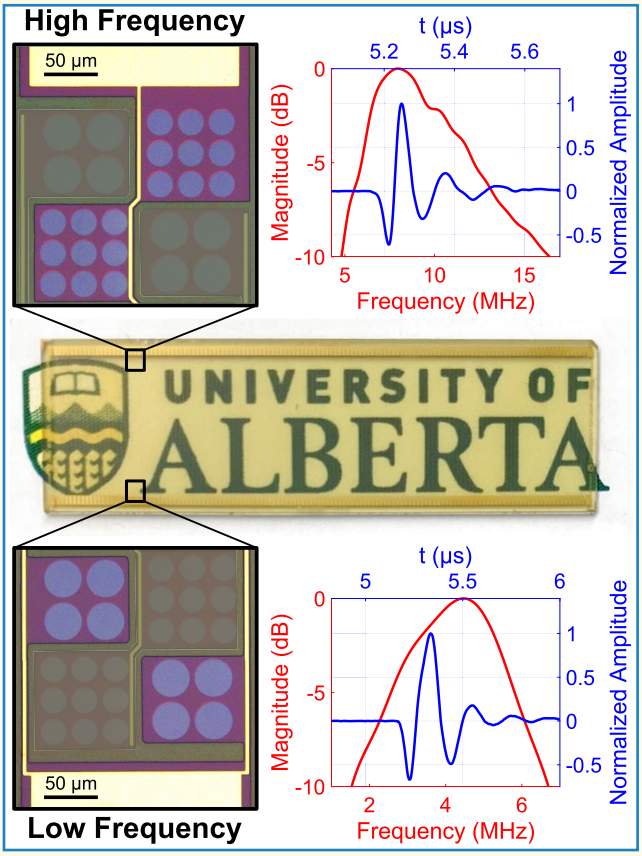

I. Introduction

PHOTOACOUSTIC imaging is a novel and powerful imaging scheme that combines both ultrasound and optical imaging techniques into one imaging modality. This imaging method takes advantage of deep ultrasound penetration and optical contrast and offers numerous biomedical applications including but not limited to hemodynamics [1], brain imaging [2], and breast cancer imaging [3]. In photoacoustic imaging, the target is illuminated with short laser pulses, after which it experiences transient thermoelastic expansion generating broadband ultrasound waves. These ultrasonic waves are then detected using an ultrasound transducer to construct the photoacoustic image of the target.

Conventional photoacoustic imaging systems use an opaque ultrasound transducer which requires the target to be illuminated in an oblique way. This configuration results in a bulky system and often requires aligning the transducer and the laser. Also, due to oblique illumination, some regions in front of the transducer are not illuminated properly by the

Manuscript received 1 September 2023; accepted 1 November 2023. Date of publication 8 November 2023; date of current version 13 December 2023. This work was supported in part by Alberta Innovates under Grant AB Innovat CASBE 212200391; in part by the Natural Sciences and Engineering Research Council of Canada (NSERC) under Grant AACASBE 567531, Grant AB Innovat AICEC 202102269, Grant RGPIN-2018-05788, and Grant AOT 567581-21; in part by the Canadian Institutes of Health Research (CIHR) under Grant PS 168936; in part by MITACS; in part by CliniSonix Inc.; and in part by NIH under Grant EITTSCA R21EYO33078 and Grant 1R21HL161626-01. *(Corresponding author: Roger Zemp.)*

The authors are with the Department of Electrical and Computer Engineering, University of Alberta, Edmonton, AB T6G 2R3, Canada (e-mail: mahyar.ghavami@ualberta.ca; rahimsob@ualberta.ca; rzemp@ualberta.ca).

Digital Object Identifier 10.1109/TUFFC.2023.3331356

Highlights

- **A transparent dual-frequency capacitive micromachined ultrasound transducer (CMUT) linear array was designed and fabricated for enhancing the performance of photoacoustic imaging systems.**
- **The transparency of the array enables through-illumination photoacoustic imaging, enhancing signal-to-noise ratio. Moreover, the dual-band operation improves both spatial resolution and imaging depth.**
- **The integration of through illumination and broadband operation in a single ultrasound transducer marks a crucial advancement, promising more compact ultrasound probe heads with superior performance.**

laser, making the imaging system blind within this region. More importantly, optical attenuation of the laser traveling a longer path compared to ultrasound waves leads to a degraded signal-to-noise ratio (SNR). These problems can be mitigated by delivering the laser light to the sample through a transparent transducer. To this end, in recent years, optically transparent piezoelectric transducers based on lithium niobate (LNO) [4], [5], [6], [7], [8], [9] or lead magnesium niobate-lead titanate (PMN-PT) [10], [11] have been proposed for through-illumination photoacoustic applications. However, limited material selection for transparent matching and backing layers worsens the fractional bandwidth and sensitivity of these types of transducers. Polyvinylidene fluoride (PVDF) polymer is another commonly used material in developing transparent piezoelectric transducers [12], [13], [14], which, due to its lower acoustic impedance, does not require matching and backing layers resulting in a wideband operation. Poor electromechanical coupling factor of PVDF-based transducers, however, limits their transmit and receive performance compared to other piezoelectric materials [15].

Capacitive micromachined ultrasound transducers (CMUTs) are another type of ultrasound transduction devices that demonstrate wider bandwidth with similar sensitivity compared to their piezoelectric counterparts. Unlike piezoelectric transducers, CMUTs are bias-sensitive and bias-switchable, which can enable bias-coded imaging schemes [16], [17], [18], [19]. CMUTs also offer more flexibility in terms of design and material selection, making them a great candidate for developing transparent ultrasound transducers. The first attempt to perform photoacoustic imaging through a CMUT device was made by Chen et al. [20] although the fabricated device was transparent only in the infrared range. Zhang et al. [21] fabricated a single-element CMUT using anodic wafer bonding, which had an improved optical transparency in the visible range. They performed through-illumination photoacoustic imaging on different imaging phantoms by mechanically scanning the transparent single-element CMUT [22]. This CMUT device, which did not have an insulation layer, was further improved by Sanders et al. [23] who developed a transparent CMUT linear array with an incorporated silicon nitride insulation layer. Zhang et al. [24] also investigated the feasibility of fabricating transparent CMUTs based on adhesive wafer bonding using both bisbenzocyclobutene (BCB) and SU-8 polymers. Ilkhechi et al. [25] fabricated a transparent CMUT linear array using an adhesive wafer bonding method, which was used for through-illumination photoacoustic imaging of wire phantoms. In another work [26], they used a similar transparent CMUT array with 128 elements for combined optical and ultrasound imaging. Recently, Ghavami et al. [27], [28] developed the first flexible variant of these optically transparent CMUT arrays and demonstrated through-illumination photoacoustic tomography on different imaging phantoms. Omidvar et al. [29] have also developed polymer-based flexible CMUT arrays that can potentially be made optically transparent for photoacoustic applications.

The fractional bandwidth of most of the transparent ultrasound transducers discussed above was below 100%. The performance of photoacoustic imaging systems largely depends on the frequency response of the ultrasound transducer. Photoacoustic signals are broadband in general, but low- and high-frequency components behave differently within the tissue. High-frequency signals provide higher spatial resolution at the expense of lower penetration depth, while low-frequency components sacrifice the resolution to provide more imaging depth. In addition, the frequency content of photoacoustic signals was shown to depend on the geometry of the absorption distribution [30]. Chee et al. [31] showed that a Gaussian-shaped absorption distribution yielded photoacoustic frequency content that scaled with the size of the distribution. Therefore, to obtain the best possible reconstruction, broadband ultrasound transducers are needed for photoacoustic imaging. Multifrequency transducers have previously been investigated to broaden the bandwidth of the ultrasound transducers [32], [33]. Due to more design flexibility and mature microfabrication techniques, micromachined ultrasound transducers have a great potential to be fabricated in multiband arrays. Chee et al. [31] fabricated a multifrequency CMUT array based on the sacrificial release method for spectroscopic photoacoustic imaging. The low- and high-frequency elements had center frequencies of 1.74 and 5.04 MHz, respectively. The dual-band operation of this device resulted in a fractional bandwidth of 170%. Zhang et al. [34] developed a photoacoustic tomography system with a multiband CMUT. The array, which was fabricated with a sacrificial release process, had center frequencies of 4 and 10 MHz. Pun et al. [35] fabricated a monolithic multiband CMUT using a standard sacrificial release process for photoacoustic computed tomography. The device consisted of five different CMUT arrays with center frequencies of 2.9, 3.7, 5.3, 7, and 9.3 MHz resulting in a fractional bandwidth

of 142% for the transducer. Wang et al. [36] developed a dual-frequency piezoelectric micromachined ultrasound transducer (PMUT) array with resonance frequencies of 1.2 and 3.4 MHz for endoscopic photoacoustic imaging.

Although having a multiband performance, the aforementioned multifrequency ultrasound transducers were opaque. Therefore, this work aims at fabrication and characterization of a transparent dual-frequency CMUT linear array for wideband through-illumination photoacoustic imaging applications. An adhesive wafer bonding method with BCB as the adhesive layer was used for the fabrication of the proposed CMUT array. The optical transparency is achieved through using indium tin oxide (ITO) as both top and bottom electrodes, and silicon nitride as the membrane material. This proposed transparent device enables light delivery through the transducer improving the SNR and image quality. Furthermore, due to its dual-band operation, deep imaging is achieved while providing fine spatial resolution.

II. Materials and Methods

A. Design

The configuration in which the low- and high-frequency elements are placed with respect to each other in a multifrequency CMUT array has been shown to affect the point spread function (PSF) of the ultrasound transducer [31]. The placement of low- and high-frequency channels with an alternating configuration imposes a larger pitch size between the elements, leading to the appearance of larger grating lobes in the receive PSF. In order to minimize the effect of these lobes, low- and high-frequency channels are designed to be in an interlaced configuration with a pitch size close to the wavelength of high-frequency elements. In past years, various models [37], [38] have been developed to predict the behavior of multifrequency CMUT arrays considering mutual acoustic impedance. In this work, the model proposed in [38] was used to design the low- and high-frequency channels to have center frequencies of 4 and 9 MHz, respectively. Considering a bandwidth of 80% for both low- and high-frequency channels, these center frequencies ensure an overlap between the frequency responses of low- and high-frequency channels, which will broaden the operational bandwidth of the device.

B. Fabrication

The proposed dual-frequency transparent CMUT array in this work was fabricated based on an adhesive wafer bonding method with four lithography steps. BCB (Cyclotene[1]4022-25 from Dupont), which is a photosensitive polymer with good thermal and chemical resistance and permanent bonding capability, has been used as the adhesive material in this process. Fig. 1 schematically shows the fabrication process with simplified top and cross-sectional views of the wafer. The fabrication process started with sputtering 250 nm of ITO on a piranha-cleaned 100-mm fused silica wafer [Fig. 1(a)]. The ITO-coated wafer was then sonicated in a bath of acetone and IPA for 10 min to ensure a clean surface for BCB application in the next step. To improve the adhesion of the BCB to the wafer, AP3000 adhesion promoter was first spin-coated on the wafer and baked at 150 °C for 60 s. Next, BCB was spin-coated onto the wafer resulting in a 350-nm layer, which defines the gap height of the CMUT cells. According to the material datasheet for Cyclotene4000 series, a film thickness of 0.8–1.8 μm can be achieved by Cyclotene4022-25. However, in this work, a thinner BCB film was achieved by employing a higher spin speed (7000 r/min) and longer spin time during the spin-coating process. To achieve thinner films, BCB can be diluted with dilution agents such as mesitylene [39]. However, the effect of the dilution should be further studied on the adhesive bonding quality. After spin coating, the BCB layer was soft baked at 60 °C for 90 s followed by a UV exposure with the first photomask to define the CMUT cavities. After a post-exposure bake at 50 °C for 60 s, the wafer was puddle developed using DS2100 developer, and the excessive developer was spun off the wafer. After drying with N_2 gas, the wafer was ready for the wafer bonding step [Fig. 1(b)]. Using an adhesive wafer bonding process with BCB acting as the adhesive material, the fused silica wafer was bonded to a 100-mm prime Si wafer with a thickness of 500 μm, on which a 700-nm low-stress silicon nitride layer had been previously deposited using low pressure chemical vapor deposition (LPCVD). Prior to the bonding step, the Si wafer was cleaned using piranha solution to minimize the contaminants on its surface. The wafer bonding step was performed using a SUSS bonder (ELAN CB6L). First, the process chamber was pumped down to 0.5 mTorr with the wafers separated by spacers to achieve vacuum-sealed cavities. The spacers were then removed bringing the wafers into contact with each other, which were then subjected to a compressive pressure of 0.5 MPa while keeping them at 150 °C for 15 min and then at 250 °C for 60 min [Fig. 1(c)]. After the bonding step, the silicon nitride on the backside of the Si wafer was etched using reactive ion etching (RIE) with CF_4 and O_2 gases, exposing the Si handle. To etch this thick Si layer, a combination of dry and wet etching processes was used in order to accelerate the process. First, the 500-μm Si handle was etched down to 150 μm using inductively coupled plasma reactive ion etching (ICPRIE) with SF_6 as the source gas. The remaining Si layer on the wafer was then wet etched using KOH at 85 °C with the silicon nitride layer underneath as the etch stop [Fig. 1(d)]. Next, another layer of ITO was sputtered onto the silicon nitride layer, which was then patterned using the second photomask and etched with HCl acid to form the top electrodes. As shown in Fig. 1(e), the top electrodes are patterned in a way to electrically isolate low- and high-frequency channels. In the next step, both silicon nitride and BCB layers were etched using RIE with SF_6 and O_2 as the source gases to access the bottom electrode [Fig. 1(f)]. At this point, a functional dual-frequency transparent CMUT array was achieved. However, the high resistance of top ITO electrodes has been shown to reduce the acoustic sensitivity along the channels [40]. To address this issue, similar to our previous works [25], [28], thin strips of Cr/Cu/Cr/Au layer stack with thicknesses of 20/600/20/150 nm were evaporated and patterned on the wafer

[1]Trademarked.

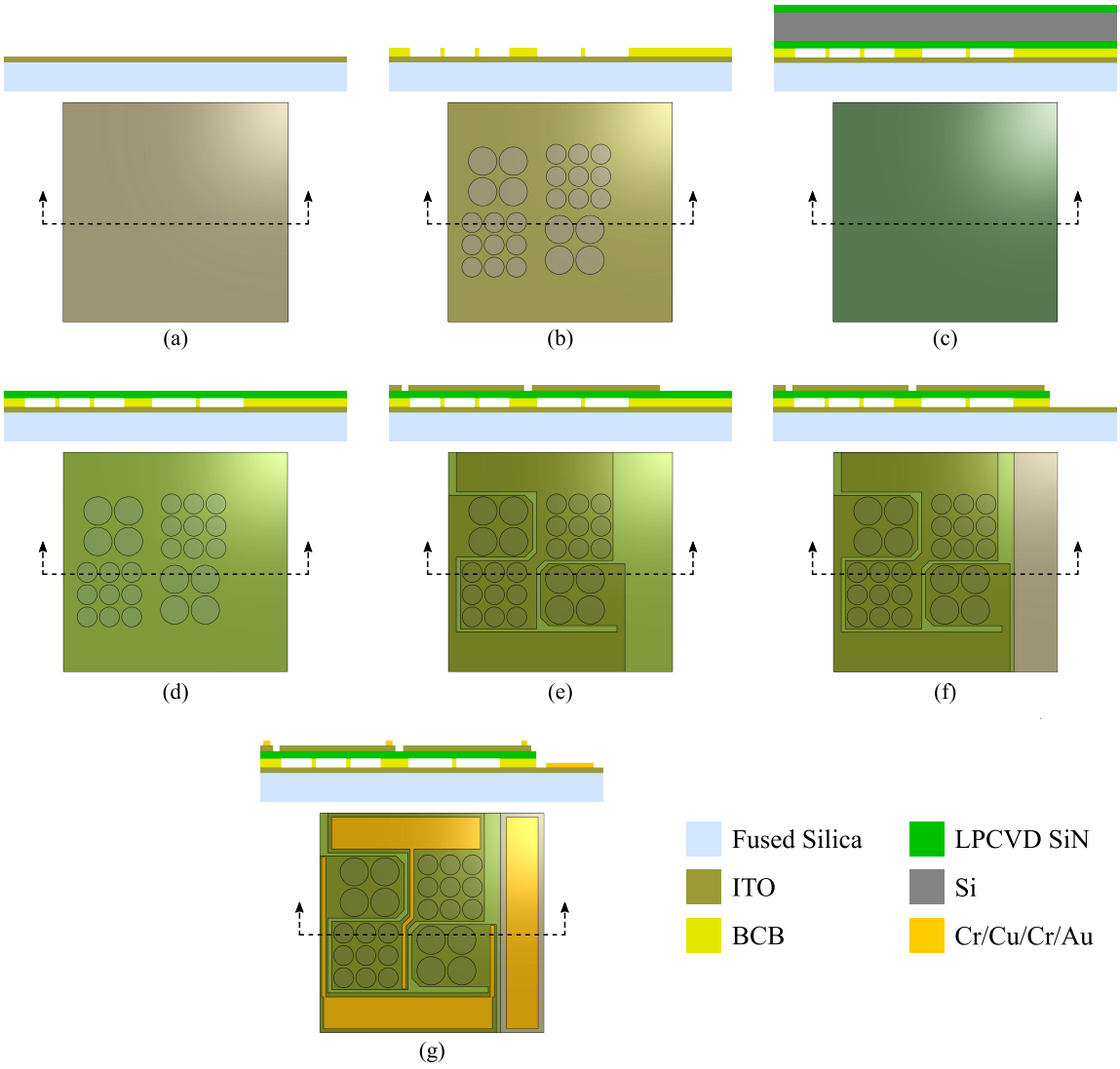

Fig. 1. Simplified schematic of the fabrication process for the proposed dual-frequency transparent CMUT arrays. (a) ITO-coated fused silica wafer. (b) Patterned BCB layer defining the CMUT cell cavities. (c) Adhesive bonding of the fused silica wafer to a silicon wafer with low-stress LPCVD silicon nitride layer. (d) Etching silicon handle using ICPRIE and KOH. (e) Sputtering and patterning of ITO for the top electrodes. (f) Etching BCB and silicon nitride using RIE to access the bottom electrode. (g) Cr/Cu/Cr/Au evaporation and liftoff.

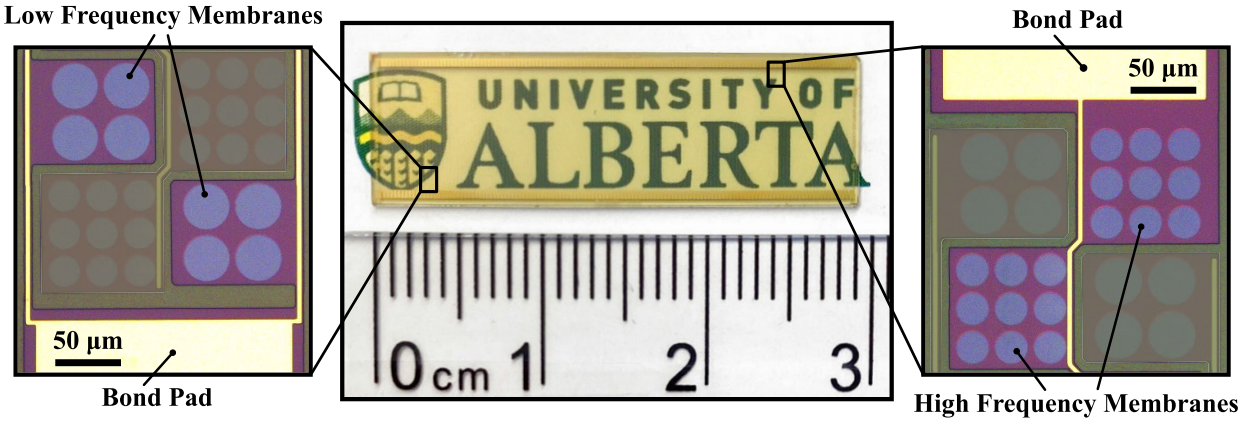

Fig. 2. Photograph of the fabricated dual-frequency transparent CMUT array in the middle with the optical microscope images showing a low-frequency channel on the left (high-frequency membranes are faded) and a high-frequency channel on the right (low-frequency membranes are faded).

using the liftoff technique [Fig. 1(g)]. With minimal effect on the optical transparency of the array, these thin metal strips not only improve the conductivity of the top electrodes but also enable wire bonding the device to a printed circuit board (PCB). The physical properties of the fabricated CMUTs are given in Table I.

TABLE I
PHYSICAL PROPERTIES OF THE FABRICATED DUAL-FREQUENCY TRANSPARENT CMUT ARRAYS

Parameter	Value
Low Frequency membrane diameter	35.5 μm
High Frequency membrane diameter	25 μm
Silicon nitride thickness (Membrane)	700 nm
BCB thickness (Gap)	350 nm
ITO thickness	250 nm
Cr/Cu/Cr/Au thickness	20/600/20/150 nm
Number of low frequency channels	128
Number of high frequency channels	128
Pitch	219 μm
Element height	7.2 mm

C. Encapsulation

To interface the fabricated CMUT array to the receive electronics, which will be discussed in more detail in Section III, the device is wire-bonded to a custom-designed PCB. For biomedical applications, CMUTs require an encapsulation layer to safeguard the patient from high voltages, as well as to protect the device from potential external damage. In research settings, CMUTs are preferred to be characterized in water, which is similar to tissue in terms of both acoustic and electrical conduction properties. The exposed electrodes of the fabricated devices in the current work, however, would prevent operating the CMUT in water due to the possibility of short circuit. Therefore, extra measures are taken to add an encapsulation layer to the fabricated CMUT arrays. First, in order to protect the wires from potential disconnection or external damage, they were covered by a mixture of 3-μm alumina powder (Logitech Ltd., Glasgow, Scotland, U.K.) and epoxy (EPO-TEK 301) with 5:4 weight ratio. After curing for 24 h at room temperature, a surface encapsulation layer could be applied onto the device. Two of the most commonly used materials that have been used for CMUT encapsulation are Parylene-C and polydimethylsiloxane (PDMS) [41]. In this work, PDMS polymer, which is a biocompatible and transparent polymer with an acoustic impedance similar to tissue, was used as the surface encapsulation material. To this end, PDMS was prepared by mixing the elastomer base (Sylgard 184 Silicone Elastomer) and the curing agent in a 10:1 weight ratio. After degassing for 30 min inside a vacuum chamber, the PMDS mixture was spin-coated on the array, followed by curing for 48 h in room temperature, which resulted in a 100-μm insulation layer.

III. RESULTS

A. Transparency

The photograph of the fabricated CMUT array is given in Fig. 2 showing its transparency in visible light. The optical microscope images of the low- and high-frequency channels with their bond pads are also shown in Fig. 2. The images depict a low-frequency channel (with faded high-frequency elements) on the left and a high-frequency channel (with faded low-frequency elements) on the right. The optical transparency of the array was measured using a Hitachi U-3900H spectrophotometer over the visible-to-near-infrared range, which is given in Fig. 3. A maximum transparency of 76.8% was achieved with the fabricated array in the visible range. The array has also a transparency of 65.9% at 532 nm, which is the wavelength of the laser pulses used in the photoacoustic experiments in this work. The fluctuations in the transparency measurement arise from the light interference within the thin films constructing the device.

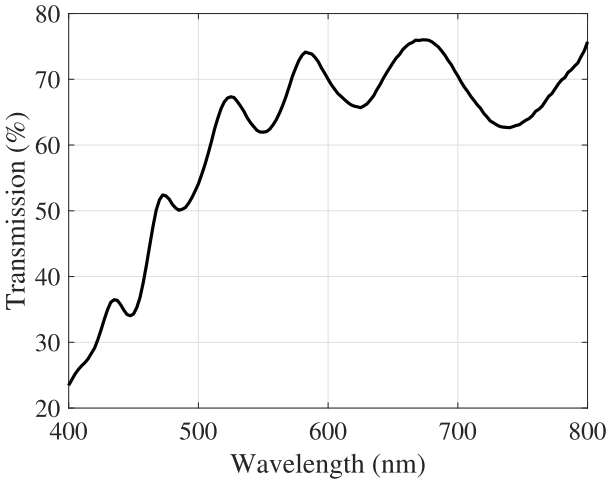

Fig. 3. Optical transparency of the fabricated dual-frequency transparent CMUT arrays measured as a function of wavelength.

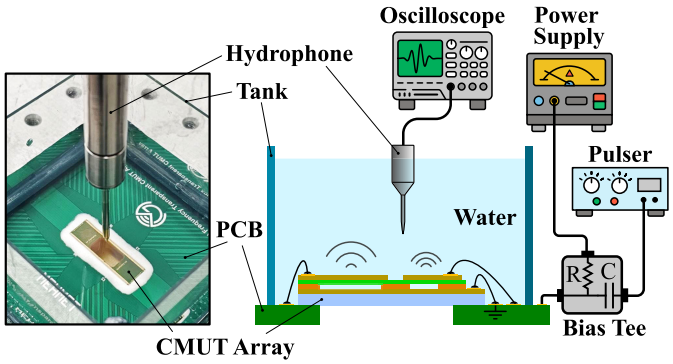

Fig. 4. Experimental setup used for hydrophone measurements on the fabricated dual-frequency transparent CMUT array.

B. Acoustic Characterization

The frequency response of the dual-frequency fabricated CMUT array was obtained by performing transmit experiments on both low- and high-frequency channels. To this end, a 3-D printed tank with glass sidewalls was then mounted on the PCB on which the array was wire bonded in order to hold water as the acoustic medium. In an experimental setup schematically shown in Fig. 4, an individual CMUT element was actuated using a pulser with the bias voltage provided to the CMUT by a dc power supply through a bias tee. The transmitted ultrasound waves by the CMUT element were then measured using a needle hydrophone, which were then recorded on an oscilloscope. This experiment was performed separately for both low- and high-frequency channels with applied bias voltages of 70 and 150 V, respectively.

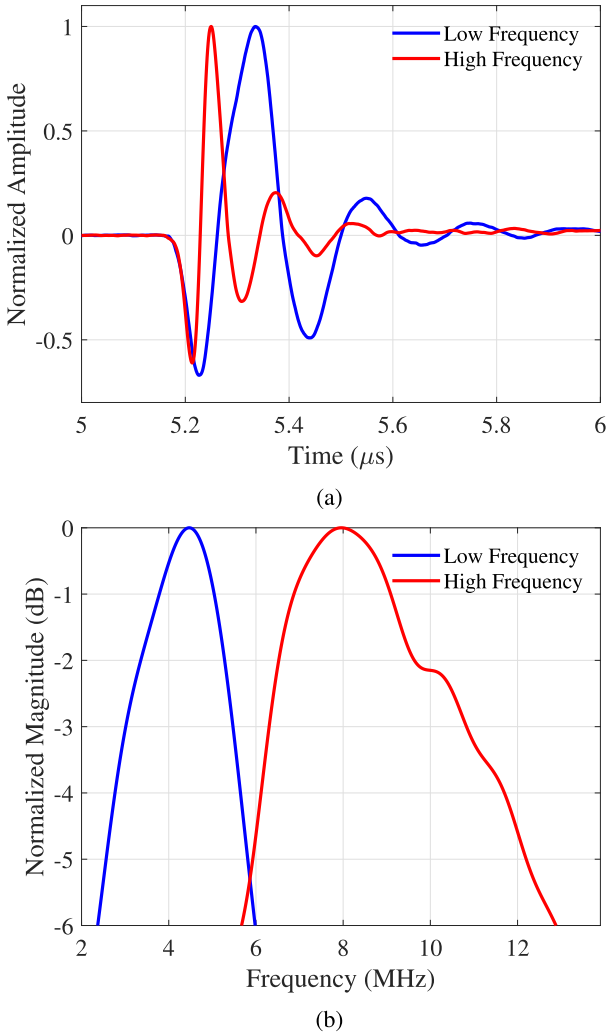

Fig. 5. Hydrophone measurements on the transmitted ultrasound using both low- and high-frequency channels of the fabricated CMUT array. (a) Temporal normalized measured signals. (b) Frequency response of the measured signals.

Fig. 5(a) shows the smoothed normalized transmitted signals by both channels recorded by the hydrophone. The transmit signals in frequency domain are obtained by taking the fast Fourier transform of the temporal signals, which are plotted in Fig. 5(b). The frequency response of the fabricated device is summarized in Table II. The fractional bandwidth of the channels was calculated based on −6- and −3-dB cutoff frequencies for one- and two-way acoustic responses, respectively. It should be noted that the axial resolution of a photoacoustic imaging system is determined by the one-way bandwidth of the ultrasound receiver [42]. The fabricated dual-frequency CMUTs operating as a single array improved the −6-dB fractional bandwidth compared to low-frequency-only elements by 60%. Compared to high-frequency-only elements, the fractional bandwidth of the dual-frequency array was 79% greater.

C. Photoacoustic Imaging

The performance of the fabricated transparent dual-frequency CMUT array was tested for through-illumination photoacoustic imaging. Fig. 6 schematically shows the

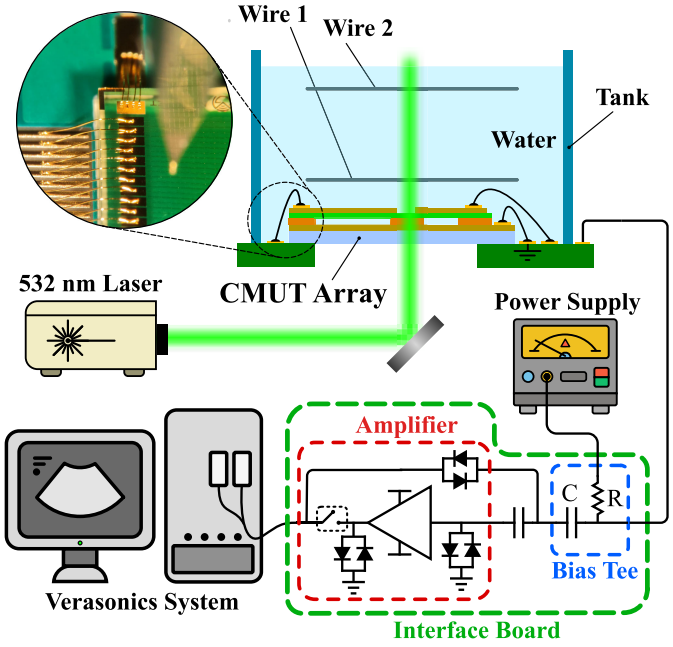

Fig. 6. Experimental setup used for through-illumination photoacoustic imaging using the fabricated CMUT array.

experimental setup for photoacoustic imaging. Using an interface board that has a dedicated bias tee and preamplification stage for each individual CMUT channel, the PCB to which the array was wire bonded was connected to a Verasonics system for data acquisition. The detailed information on this interface board design can be found in [43]. The bias voltage of the CMUT elements was also provided by a dc power supply through the bias tees on the interface board. The imaging target consisted of two aluminum wires of 100 μm in diameter, which were suspended above the array at two different depths. To perform the photoacoustic imaging, 532-nm laser pulses with 10-Hz repetition rate (Continuum Surelite III) illuminated the wire targets through the transparent CMUT array with normal incident. The incident laser fluence was 11.7 mJ/cm^2, which was lower than the American National Standards Institute (ANSI) limit of 20 mJ/cm^2 for safe laser illumination on human body [20]. With bias voltages of 50 and 100 V for low- and high-frequency channels, respectively, the photoacoustic signals are received by the array and beamformed using the back projection algorithm to reconstruct the photoacoustic images.

Fig. 7 shows the photoacoustic images of the wire targets acquired by both channels of the fabricated dual-frequency CMUT array with 40-dB dynamic range. Fig. 8 shows the axial and lateral PSFs of wire 1 acquired by low- and high-frequency channels. The spatial resolution based on full-width at half maximum (FWHM) as well as the SNR of the acquired photoacoustic images are given in Table III. The low-frequency channels of the CMUT array give a higher SNR for the deeper target due to less acoustic attenuation. On the other hand, better lateral and axial resolutions are achieved by high-frequency elements. This emphasizes the importance of having a dual-band ultrasound transducer in photoacoustic imaging systems to both maintain a deep imaging depth and fine resolution at the same time, which may not be possible with single-frequency arrays.

TABLE II
FREQUENCY RESPONSE OF THE FABRICATED DUAL-FREQUENCY TRANSPARENT CMUT ARRAY

Operation	Center Frequency	Fractional Bandwidth (-3 dB)	Fractional Bandwidth (-6 dB)
Low Frequency	4.2 MHz	59%	86%
High Frequency	9.3 MHz	54 %	77%
Dual Frequency	7.6 MHz	No overlap between bands	138%*

*There is a sensitivity gap in the mid-band which, however, is above the -6 dB threshold.

TABLE III
COMPARISON OF THE PHOTOACOUSTIC IMAGES ACQUIRED BY LOW- AND HIGH-FREQUENCY CHANNELS OF THE FABRICATED CMUT ARRAY IN TERMS OF SPATIAL RESOLUTION AND SNR

Channel	Axial Resolution (μm)		Lateral Resolution (μm)		SNR (dB)	
	Wire 1	Wire 2	Wire 1	Wire 2	Wire 1	Wire 2
Low Frequency	477	478	326	891	48.97	47.67
High Frequency	325	388	212	501	37.52	33.39

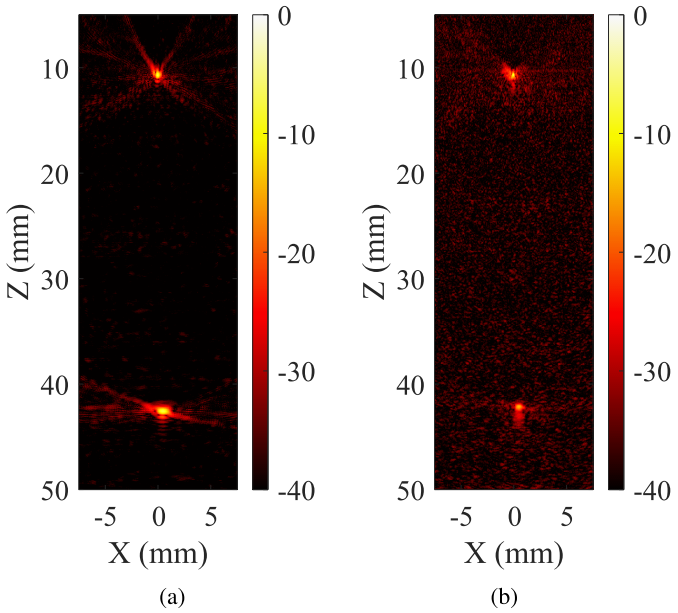

Fig. 7. Photoacoustic image of aluminum wire targets acquired by (a) low- and (b) high-frequency channels of the fabricated CMUT array with 40-dB dynamic range.

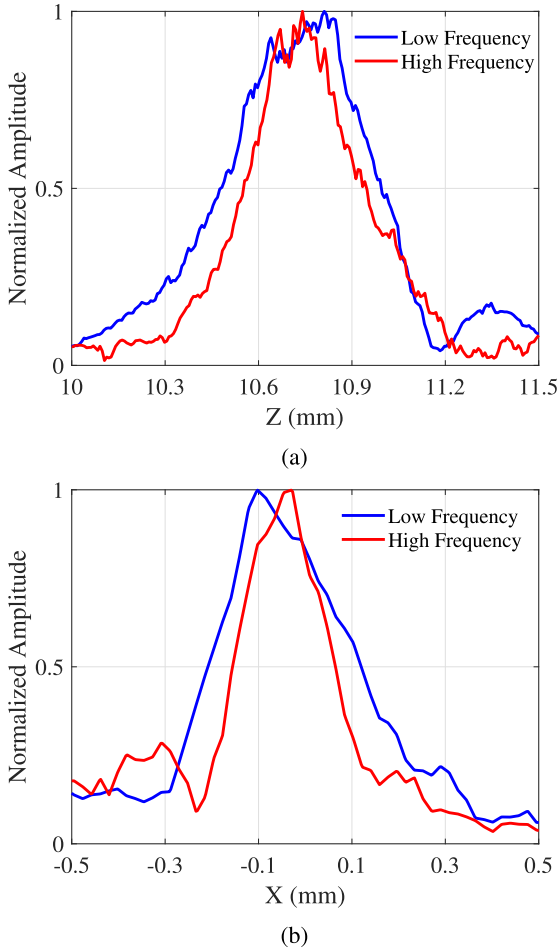

Fig. 8. PSF of low- and high-frequency channels of the fabricated CMUT array measured based on the first wire: (a) axial resolution and (b) lateral resolution.

IV. DISCUSSION

Transparent ultrasound transducers are becoming more popular as they enable efficient light delivery to the target through the transducer in photoacoustic applications, resulting in improved image quality and more compact systems. This work introduces a transparent CMUT linear array with dual-frequency operation for wideband photoacoustic imaging applications. The device was fabricated on a fused silica wafer using an adhesive wafer bonding process with four lithography steps. Optical transparency was achieved by using BCB as the adhesive and sidewall material, ITO as the top and bottom electrodes, and silicon nitride as the CMUT membranes. To maintain a consistent sensitivity along the CMUT elements, the conductivity of the top ITO electrodes was further improved by patterning thin Cr/Cu/Cr/Au metal stack strips with minimal effect on the device transparency. The low- and high-frequency channels, which were measured to have center frequencies of 4.2 and 9.3 MHz, respectively, resulted in a wider bandwidth for the device compared to single-frequency cases. Finally, the fabricated transparent array was used in through-illumination photoacoustic imaging of wire phantoms suspended at different depths above the array to evaluate the performance of both channels. Comparing the photoacoustic images acquired by low- and high-frequency subarrays, it was seen that the dual-band performance of the fabricated transparent CMUT array could

maintain both deeper imaging depth and finer spatial resolution in through-illumination photoacoustic imaging compared to single-frequency operation.

In the fabricated CMUT array, the low- and high-frequency elements were designed to be in an interlacing configuration, which has been shown to improve the spatial resolution by minimizing the grating lobes [31]. However, this architecture sacrifices the active area of the elements in order to maintain a smaller pitch between the transducer elements. In addition, mutual acoustic impedance effects can be more pronounced due to the low- and high-frequency channels being closer to each other.

Although the low- and high-frequency channels of the fabricated CMUT array have overlapping frequency bands within −6 dB, the receive sensitivity is not necessarily uniform within this frequency range. However, it has been shown that the relative sensitivity of these low- and high-frequency channels with complementary frequency bands can be calibrated and applied to the channel data to closely mimic a single wideband transducer [44]. This is important in achieving quantitative functional photoacoustic images to account for the differences in sensitivity of the dual-frequency subarrays.

As reported by Zhang et al. [22], the laser illumination through a transparent transducer can generate photoacoustic signals due to the optical absorption of the array, and the resulting echoes reflected from the imaging target can contaminate the receive signals. The photoacoustic signal generated due to the optical absorption of the fabricated transparent CMUTs was characterized by performing through-illumination photoacoustic imaging on a single wire target. Fig. 9(a) shows the tenfold averaged receive signal as a function of sample number from a low-frequency element of the transparent dual-frequency CMUT array. The photoacoustic signal of the array reflected from the wire target is expected to appear at double the propagation time as the photoacoustic signal from the wire target. However, as it can be seen from Fig. 9(a), at around twice the sample number, the photoacoustic signal is received from the wire, and the signal fluctuates at the noise level of the channel data. Considering the higher optical transparency of the fabricated array compared to [22] and the difference in the receive electronics, we speculate that the strength of the photoacoustic signals generated from the fabricated arrays was within the noise level. In order to further minimize the effect of noise for recovering the potential coherent signal buried within the noise, a scan line from an envelope-detected B-mode photoacoustic image of the single wire target is also given in Fig. 9(b), which, however, does not show any artifacts or clutters at twice the depth of the wire target. It should be noted that when beamforming is implemented to reconstruct a photoacoustic image, the delays are calculated for one-way rather than round-trip propagation. Thus, any plane-wave transmit–receive signals generated by the photoacoustic effect of the array are not coherently focused but may show up as clutter in the image. It should also be noted that a transparent transducer will absorb less of the laser light that is scattered within the tissue compared to an opaque transducer.

Target illumination through this transparent CMUT transducer has the advantage of improving the light delivery and

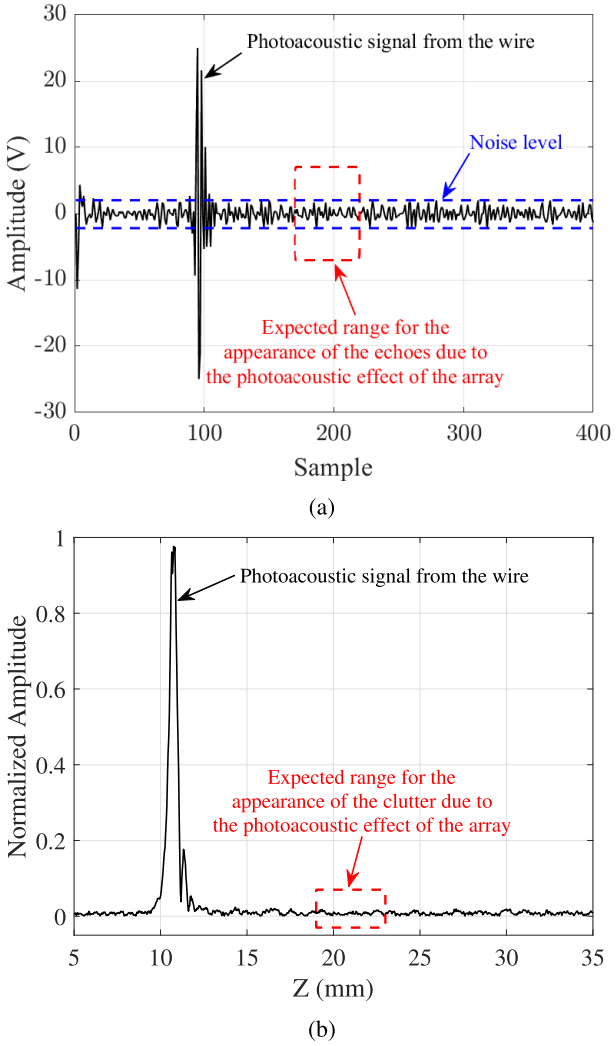

Fig. 9. Through-illumination photoacoustic imaging of a single wire target using the low-frequency channels of the fabricated transparent CMUT array. (a) Averaged receive signal by a single element. (b) Envelope-detected A-scan from the beamformed photoacoustic image of the wire target.

SNR compared to oblique illumination [25]. This can be even more beneficial in using 2-D arrays with a larger surface area in photoacoustic applications. Furthermore, CMUTs are bias-sensitive and bias-switchable, which can be utilized in fast bias-coded volumetric imaging applications using transparent row–column arrays [45], [46].

V. Conclusion

This work reports the fabrication and characterization of a dual-frequency transparent CMUT linear array, which integrates both through-illumination photoacoustic imaging and broadband operation into a single ultrasound transducer. The transparency of the array contributes to an improved SNR with the dual-band operation ensuring both high resolution and deep imaging. The fabricated transparent device, which consists of BCB as the adhesive and sidewall material, ITO as the both top and bottom electrodes, silicon nitride as the membrane, and thin metal strips for improved conductivity along top electrodes, has a maximum optical transparency of 76.8% in the visible range. The dual-frequency operation

of the array with center frequencies of 4.2 and 9.3 MHz was shown to improve the bandwidth of the device by 60% and 79% compared to low- and high-frequency-only cases, respectively. The fabricated CMUT array was used in through-illumination photoacoustic imaging of two wire phantoms at different depths. The reconstructed photoacoustic images showed that the low-frequency channels of the CMUT array provide a higher SNR at deeper depths with its high-frequency elements giving a finer spatial resolution. The proposed fabricated array can set the stage for broadband transparent row–column arrays for real-time 3-D photoacoustic imaging.

Acknowledgment

The authors are grateful for the resources supplied by CMC Microsystems Canada, Kingston, ON, Canada. They would like to thank nanoFAB facility staff at the University of Alberta, Edmonton, AB, Canada, for their technical support during the device fabrication. Also, they have used images from Flaticon.com to design the schematics of the instruments in Figs. 4 and 6.

References

[1] C. Liu and L. Wang, "Functional photoacoustic microscopy of hemodynamics: A review," *Biomed. Eng. Lett.*, vol. 12, no. 2, pp. 1–28, 2022.

[2] J. Yao and L. V. Wang, "Photoacoustic brain imaging: From microscopic to macroscopic scales," *Neurophotonics*, vol. 1, no. 1, May 2014, Art. no. 011003.

[3] A. P. Rao, N. Bokde, and S. Sinha, "Photoacoustic imaging for management of breast cancer: A literature review and future perspectives," *Appl. Sci.*, vol. 10, no. 3, p. 767, Jan. 2020.

[4] A. Dangi, S. Agrawal, and S.-R. Kothapalli, "Lithium niobate-based transparent ultrasound transducers for photoacoustic imaging," *Opt. Lett.*, vol. 44, no. 21, pp. 5326–5329, 2019.

[5] R. Chen et al., "Transparent high-frequency ultrasonic transducer for photoacoustic microscopy application," *IEEE Trans. Ultrason., Ferroelectr., Freq. Control*, vol. 67, no. 9, pp. 1848–1853, Sep. 2020.

[6] S. Park, S. Kang, and J. H. Chang, "Optically transparent focused transducers for combined photoacoustic and ultrasound microscopy," *J. Med. Biol. Eng.*, vol. 40, no. 5, pp. 707–718, Oct. 2020.

[7] J. Park et al., "Quadruple ultrasound, photoacoustic, optical coherence, and fluorescence fusion imaging with a transparent ultrasound transducer," *Proc. Nat. Acad. Sci. USA*, vol. 118, no. 11, Mar. 2021, Art. no. e1920879118.

[8] M. Chen et al., "High-speed wide-field photoacoustic microscopy using a cylindrically focused transparent high-frequency ultrasound transducer," *Photoacoustics*, vol. 28, Dec. 2022, Art. no. 100417.

[9] H. Chen et al., "A transparent ultrasound array for real-time optical, ultrasound, and photoacoustic imaging," *BME Frontiers*, vol. 2022, Jan. 2022, Art. no. 9871098.

[10] H. Chen et al., "Transparent ultrasound transducers for multiscale photoacoustic imaging," *Proc. SPIE*, vol. 11642, pp. 142–149, Mar. 2021.

[11] M. R. Sobhani, K. Latham, J. Brown, and R. J. Zemp, "Bias-sensitive transparent single-element ultrasound transducers using hot-pressed PMN-PT," *OSA Continuum*, vol. 4, no. 10, pp. 2606–2614, 2021.

[12] C. Fang, H. Hu, and J. Zou, "A focused optically transparent PVDF transducer for photoacoustic microscopy," *IEEE Sensors J.*, vol. 20, no. 5, pp. 2313–2319, Mar. 2020.

[13] Y.-H. Liu et al., "Transparent flexible piezoelectric ultrasound transducer for photoacoustic imaging system," *IEEE Sensors J.*, vol. 22, no. 3, pp. 2070–2077, Feb. 2022.

[14] H. Hu, C. Fang, and J. Zou, "An optically-transparent PVDF transducer array for photoacoustic tomography," *Proc. SPIE*, vol. 11960, pp. 338–343, 2022.

[15] D. Ren, Y. Sun, J. Shi, and R. Chen, "A review of transparent sensors for photoacoustic imaging applications," *Photonics*, vol. 8, no. 8, p. 324, Aug. 2021.

[16] C. Ceroici et al., "3D photoacoustic imaging using Hadamard-bias encoding with a crossed electrode relaxor array," *Opt. Lett.*, vol. 43, no. 14, pp. 3425–3428, 2018.

[17] C. Ceroici, K. Latham, B. A. Greenlay, J. A. Brown, and R. J. Zemp, "Fast orthogonal row–column electronic scanning experiments and comparisons," *IEEE Trans. Ultrason., Ferroelectr., Freq. Control*, vol. 66, no. 6, pp. 1093–1101, Jun. 2019.

[18] M. R. Sobhani, M. Ghavami, A. K. Ilkhechi, J. Brown, and R. Zemp, "Ultrafast orthogonal row–column electronic scanning (uFORCES) with bias-switchable top-orthogonal-to-bottom electrode 2-D arrays," *IEEE Trans. Ultrason., Ferroelectr., Freq. Control*, vol. 69, no. 10, pp. 2823–2836, Oct. 2022.

[19] A. K. Ilkhechi et al., "High-voltage bias-switching electronics for volumetric imaging using electrostrictive row–column arrays," *IEEE Trans. Ultrason., Ferroelectr., Freq. Control*, vol. 70, no. 4, pp. 324–335, Apr. 2023.

[20] J. Chen, M. Wang, J.-C. Cheng, Y.-H. Wang, P.-C. Li, and X. Cheng, "A photoacoustic imager with light illumination through an infrared-transparent silicon CMUT array," *IEEE Trans. Ultrason., Ferroelectr., Freq. Control*, vol. 59, no. 4, pp. 766–775, Apr. 2012.

[21] X. Zhang, O. Adelegan, F. Y. Yamaner, and O. Oralkan, "CMUTs on glass with ITO bottom electrodes for improved transparency," in *Proc. IEEE Int. Ultrason. Symp. (IUS)*, Sep. 2016, pp. 1–4.

[22] X. Zhang, X. Wu, O. J. Adelegan, F. Y. Yamaner, and Ö. Oralkan, "Backward-mode photoacoustic imaging using illumination through a CMUT with improved transparency," *IEEE Trans. Ultrason., Ferroelectr., Freq. Control*, vol. 65, no. 1, pp. 85–94, Jan. 2018.

[23] J. L. Sanders et al., "A handheld 1D transparent CMUT array probe for photoacoustic imaging: Preliminary results," in *Proc. IEEE Int. Ultrason. Symp. (IUS)*, Sep. 2017, pp. 1–4.

[24] X. Zhang, O. Adelegan, F. Y. Yamaner, and Ö. Oralkan, "An optically transparent capacitive micromachined ultrasonic transducer (CMUT) fabricated using SU-8 or BCB adhesive wafer bonding," in *Proc. IEEE Int. Ultrason. Symp. (IUS)*, Sep. 2017, pp. 1–4.

[25] A. K. Ilkhechi, C. Ceroici, Z. Li, and R. Zemp, "Transparent capacitive micromachined ultrasonic transducer (CMUT) arrays for real-time photoacoustic applications," *Opt. Exp.*, vol. 28, no. 9, pp. 13750–13760, 2020.

[26] A. K. Ilkhechi, C. Ceroici, E. Dew, and R. Zemp, "Transparent capacitive micromachined ultrasound transducer linear arrays for combined realtime optical and ultrasonic imaging," *Opt. Lett.*, vol. 46, no. 7, pp. 1542–1545, 2021.

[27] M. Ghavami, A. K. Ilkhechi, and R. Zemp, "Through-illumination photoacoustic imaging using flexible transparent CMUT arrays," *Proc. SPIE*, vol. 2022, Mar. 2022, Art. no. PC119602H.

[28] M. Ghavami, A. K. Ilkhechi, and R. Zemp, "Flexible transparent CMUT arrays for photoacoustic tomography," *Opt. Exp.*, vol. 30, no. 10, pp. 15877–15894, May 2022.

[29] A. Omidvar, E. Cretu, R. Rohling, M. Cresswell, and A. J. Hodgson, "Flexible PolyCMUTs: Fabrication and characterization of a flexible polymer-based capacitive micromachined ultrasonic array for conformal ultrasonography," *Adv. Mater. Technol.*, vol. 8, no. 5, Mar. 2023, Art. no. 2201316.

[30] L. V. Wang and H.-I. Wu, *Biomedical Optics: Principles and Imaging*. Hoboken, NJ, USA: Wiley, 2012.

[31] R. K. W. Chee, P. Zhang, M. Maadi, and R. J. Zemp, "Multifrequency interlaced CMUTs for photoacoustic imaging," *IEEE Trans. Ultrason., Ferroelectr., Freq. Control*, vol. 64, no. 2, pp. 391–401, Feb. 2017.

[32] A. Kshirsagar et al., "Multi-frequency CMUT arrays for imaging-therapy applications," in *Proc. IEEE Int. Ultrason. Symp. (IUS)*, Jul. 2013, pp. 1991–1993.

[33] J. Yang et al., "Characterization of an array-based dual-frequency transducer for superharmonic contrast imaging," *IEEE Trans. Ultrason., Ferroelectr., Freq. Control*, vol. 68, no. 7, pp. 2419–2431, Jul. 2021.

[34] J. Zhang et al., "Development of a multi-band photoacoustic tomography imaging system based on a capacitive micromachined ultrasonic transducer array," *Appl. Opt.*, vol. 56, no. 14, pp. 4012–4018, 2017.

[35] S. H. Pun et al., "Monolithic multiband CMUTs for photoacoustic computed tomography with in vivo biological tissue imaging," *IEEE Trans. Ultrason., Ferroelectr., Freq. Control*, vol. 65, no. 3, pp. 465–475, Mar. 2018.

[36] H. Wang, P. X.-L. Feng, and H. Xie, "A high-density and dual-frequency PMUT array based on thin ceramic PZT for endoscopic photoacoustic imaging," in *Proc. IEEE 34th Int. Conf. Micro Electro Mech. Syst. (MEMS)*, Jan. 2021, pp. 891–894.

[37] S. Satir, J. Zahorian, and F. L. Degertekin, "A large-signal model for CMUT arrays with arbitrary membrane geometry operating in non-collapsed mode," *IEEE Trans. Ultrason., Ferroelectr., Freq. Control*, vol. 60, no. 11, pp. 2426–2439, Nov. 2013.

[38] M. Maadi and R. J. Zemp, "Self and mutual radiation impedances for modeling of multi-frequency CMUT arrays," *IEEE Trans. Ultrason., Ferroelectr., Freq. Control*, vol. 63, no. 9, pp. 1441–1454, Sep. 2016.

[39] G. P. Lavallee, J. M. Catchmark, and Y. Lee, "Patterning compositions using e-beam lithography and structures and devices made thereby," U.S. Patent 6 919 164, Jul. 19, 2005.

[40] A. S. Havreland, M. Engholm, B. G. Tomov, J. A. Jensen, O. Hansen, and E. V. Thomsen, "CMUT electrode resistance design: Modeling and experimental verification by a row-column array," *IEEE Trans. Ultrason., Ferroelectr., Freq. Control*, vol. 66, no. 6, pp. 1110–1118, Jun. 2019.

[41] J. Oevermann, P. Weber, and S. H. Tretbar, "Encapsulation of capacitive micromachined ultrasonic transducers (CMUTs) for the acoustic communication between medical implants," *Sensors*, vol. 21, no. 2, p. 421, Jan. 2021.

[42] H. Chen et al., "Optical-resolution photoacoustic microscopy using transparent ultrasound transducer," *Sensors*, vol. 19, no. 24, p. 5470, Dec. 2019.

[43] B. A. Greenlay, "Fabrication and integration of CMUT sensors," Ph.D. dissertation, Dept. Elect. Comput. Eng., Univ. Alberta, Edmonton, AB, Canada, 2017.

[44] S. Chandramoorthi, J. J. M. Riksen, A. V. Nikolaev, A. F. W. Van Der Steen, and G. Van Soest, "Wideband photoacoustic imaging in vivo with complementary frequency conventional ultrasound transducers," *Frontiers Phys.*, vol. 10, p. 991, Oct. 2022.

[45] M. Ghavami, M. R. Sobhani, and R. Zemp, "Transparent row-column CMUT arrays for volumetric photoacoustic imaging," *Proc. SPIE*, vol. 12631, pp. 50–54, Aug. 2023.

[46] M. R. Sobhani, M. Ghavami, and R. Zemp, "Bias-sensitive 128×128 hand-held TOBE ultrasound probe based on electrostrictive PMN-PT for photoacoustic applications," *Proc. SPIE*, vol. 12631, pp. 73–75, Aug. 2023.

Mahyar Ghavami (Graduate Student Member, IEEE) was born in Tabriz, Iran. He received the B.Sc. degree (Hons.) in mechanical engineering from the University of Tabriz, Tabriz, in 2014, and the M.Sc. degree (Hons.) in mechanical engineering from Tarbiat Modares University, Tehran, Iran, in 2017. He is currently pursuing the Ph.D. degree in Dr. Zemp's research group with the Department of Electrical and Computer Engineering, University of Alberta, Edmonton, AB, Canada.

His research focuses on the development of ultrasound transducers for biomedical applications.

Mr. Ghavami is a holder of the Alberta Graduate Excellence Scholarship (AGES).

Mohammad Rahim Sobhani (Graduate Student Member, IEEE) was born in Tabriz, Iran. He received the B.Sc. degree (Hons.) in biomedical engineering (bioelectric) from the Sahand University of Technology, Tabriz, Iran, in 2012 and the M.Sc. degree in electrical and electronics engineering from Ozyegin University, Istanbul, Turkey, in 2015. He is currently pursuing the Ph.D. degree with the Department of Electrical and Computer Engineering, University of Alberta, Edmonton, AB, Canada.

His current research interests include the development of opaque/transparent large-area electrostrictive top-orthogonal-to-bottom electrode (eTOBE) arrays, ultrasound front-end electronics, and microfabrication.

Roger Zemp (Member, IEEE) was born in Calgary, AB, Canada, in 1974. He received the B.Sc. degree in physics from the University of Alberta, Edmonton, AB, Canada, in 1998, the M.A.Sc. degree in electrical and computer engineering from the University of Toronto, Toronto, ON, Canada, in 2000, and the Ph.D. degree in biomedical engineering from the University of California at Berkeley, Berkeley, CA, USA, in 2004.

From 2004 to 2006, he was with Texas A&M University, College Station, TX, USA, as a Postdoctoral Fellow. He was with Washington University, St. Louis, MO, USA, from 2006 to 2007. He is currently a Professor with the Department of Electrical and Computer Engineering, University of Alberta. His current research interests include ultrasound imaging, biomedical optics, and photoacoustic imaging.